Normal incidence detection of ultraviolet, visible, and mid-infrared radiation in a single GaAs/AlGaAs device

G. Ariyawansa,[1] P. V. V. Jayaweera,[1] A. G. U. Perera,[1,2,*] S. G. Matsik,[2] M. Buchanan,[3] Z. R. Wasilewski,[3] and H. C. Liu[3]

[1]*Department of Physics and Astronomy, Georgia State University, Atlanta, Georgia 30303, USA*
[2]*NDP Optronics LLC, Mableton, Georgia 30126, USA*
[3]*Institute for Microstructural Sciences, National Research Council, Ottawa, Ontario K1A 0R6, Canada*
[*]*Corresponding author: uperera@gsu.edu*

Received March 27, 2009; revised May 12, 2009; accepted May 15, 2009;
posted June 2, 2009 (Doc. ID 109395); published June 29, 2009

A GaAs/AlGaAs detector is demonstrated showing multiple detection capabilities. This detector exhibits a broad spectral response in the 200–870 nm (ultraviolet–visible) range for forward bias and in the 590–870 nm (visible) range for reverse bias. In the mid-IR region, two peaks at 5 and 8.9 μm can be observed for low and high forward bias voltages, respectively. In addition, the peak at 8.9 μm is sensitive to the polarization of the incoming radiation. © 2009 Optical Society of America

OCIS codes: 040.3060, 040.5160, 040.7190, 230.0040, 230.0250, 250.0040.

GaAs has become one of the most matured materials for the development of IR devices, especially IR photodetectors. Photodetectors [1–3] as well as dual-band focal plane arrays (FPAs) [4] have been successfully developed, utilizing various device architectures such as quantum well, free-carrier-based structures, and intrinsic detectors. Despite the interest in GaAs material for IR devices, researchers have not paid much attention on the use of GaAs for the detection of visible (VIS) or UV radiation. One possible reason would be the availability of wide-bandgap materials for the UV region and Si and InGaAs for the VIS region. However, for detectors sensitive in all of the three regions, GaAs has many advantages compared with other materials. One of the advantages is that the extension to array detectors should be a relatively straightforward process since the GaAs/AlGaAs material system is well developed. Here, a GaAs/AlGaAs quantum-well IR photodetector (QWIP) is reported, showing response bands in the UV–VIS (200–870 nm) and the mid-IR (MIR) (5 and 8.9 μm) under normal incidence configuration. This structure provides wavelength selectivity based on the magnitude of the applied bias voltage. Normal incidence detection was achieved using a metal grating fabricated on the structure, which also leads to polarization sensitivity. While multicolor IR detection [5–8] enables the generation of a complete thermal map of scenes, the polarization information [9] provides the surface features, shape, shading, and roughness, which can be used for target recognition.

The multiband detector demonstrated here was grown by molecular beam epitaxy and resembles a p-i-n structure with a p-type QWIP, i-GaAs region, and an n-type QWIP. As schematically shown in Fig. 1, the three regions are sandwiched between a highly doped p-type top and an n-type bottom contact regions. The p-type QWIP region consists of 40 periods of 3.1-nm-thick GaAs wells in 25-nm-thick $Al_{0.55}Ga_{0.45}As$ barriers, and it was designed to respond around 5 μm. The n-type QWIP region consists of 50 periods of 5.4-nm-thick GaAs wells in 40-nm-thick $Al_{0.24}Ga_{0.76}As$ barriers, and it was designed to respond around 9 μm. To couple normal incidence light with the n-type QWIP, a 1D metal grid having a fill factor of 0.5 and a grating period of 2.8 μm (corresponding to the first-order diffraction peak at 9 μm) was fabricated on the top of the structure.

The band diagram under zero applied bias (ignoring the band bending at the interfaces), showing both valence and conduction bands along with the calculated bound states in the two QWIP regions is shown in Fig. 2(a). Under forward and reverse bias conditions, this detector structure behaves similar to a regular p-i-n photodetector, except that the operation of the two QWIPs is more prominent under forward bias (top-contact positive). Under reverse bias, the excited electrons in the n-QWIP and the holes in the p-QWIP should transport toward the bottom and top

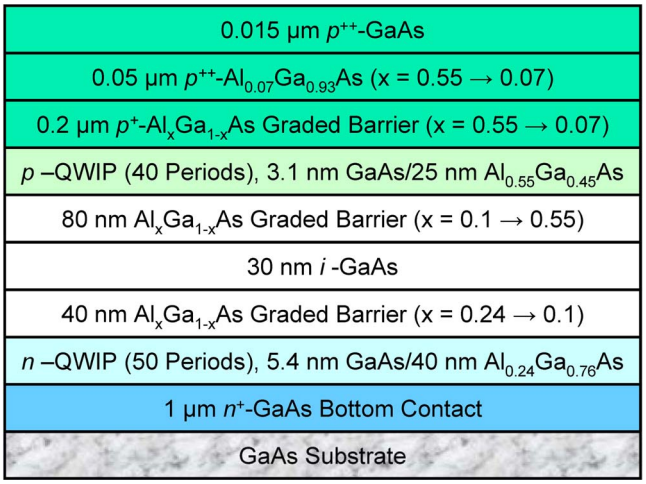

Fig. 1. (Color online) Schematic structure of the GaAs-based detector. This structure consists of a p-type QWIP (5 μm) at the top, an intrinsic GaAs region (middle), and an n-type QWIP (9 μm) at the bottom.

0146-9592/09/132036-3/$15.00

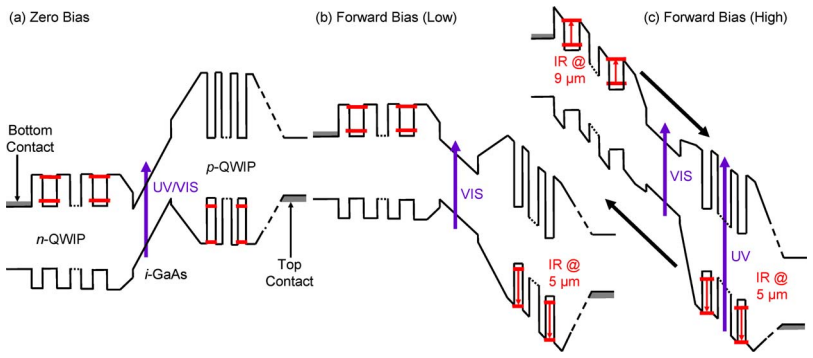

Fig. 2. (Color online) Conduction and valence band profiles of the detector at (a) zero bias, (b) low forward bias (top-contact positive), and (c) high forward bias. Note that the band bending affects at the interfaces are not shown to reduce the complexity. Interband transitions across the bandgap leads to UV–VIS detection, while electron intersubband transitions in the two QWIP regions lead to two-color IR detection.

contacts, respectively, to generate a photocurrent. This photocarrier transport mechanism is not favorable owing to the trapping of electrons at the $Al_{0.55}Ga_{0.45}As$ layer/top-contact interface and holes at the $Al_{0.24}Ga_{0.76}As$/bottom-contact interface. Also, the extremely low dark current (tunneling current) under reverse bias reduces the refilling of the well ground states. However, under forward bias (top-contact positive), the transport of electrons is from the n to the p region, while the holes travel from the p to the n region. Since the photoexcited electrons and holes in the two QWIPs also follow this, as illustrated in Fig. 2(c), the photocurrent generation is prominent under forward bias.

The dark current density of the detector measured at 80 and 300 K is shown in Fig. 3(a), indicating a very low reverse dark current and dramatic dark current increase in the forward direction. Based on calculations [10], an interband absorption coefficient

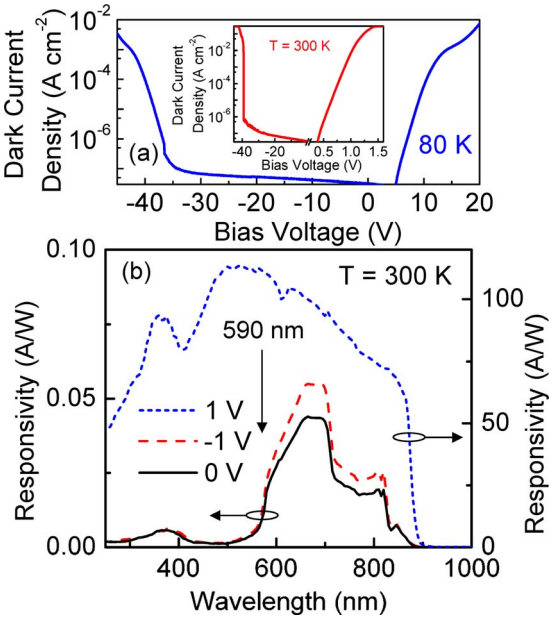

Fig. 3. (Color online) (a) Dark current density of the detector measured at 80 and 300 K, clearly showing characteristics of a p-i-n photodetector. (b) Interband responsivity of the detector showing a threshold at ~870 nm (corresponding to the GaAs direct bandgap at 300 K) under −1, 0, and 1 V bias at 300 K.

greater than 10^5 cm^{-1} for GaAs can be obtained for wavelengths below ~870 nm, which corresponds to the direct bandgap, indicating the potential for UV/VIS detection in GaAs. The calibrated spectral responsivity at −1, 0, and 1 V bias values at 300 K is shown in Fig. 3(b). At 1 V bias, a high responsivity (~92 A/W) was observed, probably owing to high photoconductive gain [11]. The detectivity (D^*) at 700 nm under −1 V is $\sim 1.8\times10^{14}$ Jones. Despite the high responsivity, a lower D^* of $\sim 2\times10^{11}$ Jones was observed at 1 V bias owing to the higher noise current compared with that at −1 V. While it is clear that the threshold at 870 nm corresponds to the fundamental bandgap of GaAs, there is also a clear threshold at 590 nm, which is specific to this particular detector structure and corresponds to the bandgap of $Al_{0.55}Ga_{0.45}As$. According to Fig. 2(a), a photocurrent generation is possible only in the intrinsic GaAs region (i region) at zero bias, since the excited carrier collection takes place owing to the build-in potential. However, light passing through the top p-QWIP region with energy greater than the bandgap of the undoped $Al_{0.55}Ga_{0.45}As$ is absorbed owing to the strong interband transitions in $Al_{0.55}Ga_{0.45}As$ layers (note that the interband transitions in the p-doped GaAs wells is not very efficient). Also, these excited electron–hole pairs do not contribute to the photocurrent. Hence, no response was observed below 590 nm at zero bias. This process is the same for reverse applied bias, since the applied electric field appears mostly across the i region. However, as seen in Fig. 3(b), a broad response from 200–870 nm was observed under forward bias. This is because the electron–hole pairs generated in the i-GaAs region and the top $Al_{0.55}Ga_{0.45}As$ layers can be collected as shown by the arrows in Fig. 2(c).

As shown in Fig. 4(a), two peaks in the MIR region appear at 5 μm (p-QWIP) and 8.9 μm (n-QWIP) at 80 K for unpolarized normal incidence radiation. The responsivity of the two peaks depends on the strength of the applied bias. As shown in the inset to Fig. 4(a), the peak at 5 μm is dominant at low bias (10 V), while the peak at 8.9 μm is dominant at high bias (15 V). This bias dependency of the two response peaks agrees with the concept explained elsewhere [12] for a multicolor detector consisting of three QWIP

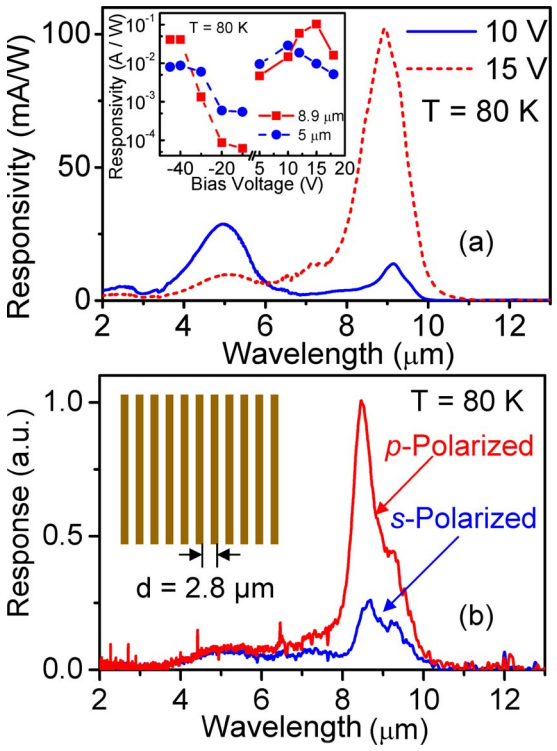

Fig. 4. (Color online) (a) Two-color IR response at 80 K. Variation in the responsivity for the two peaks with bias is shown in the inset. (b) Response for *s*- and *p*-polarized light, showing a 100:25 polarization extinction ratio. Schematics of the 1D metal grid fabricated on the detector, having a metal-open pattern (with a fill factor of 0.5) with a grating period of 2.8 μm, is shown in the inset.

stacks. When two QWIP structures, which respond to different wavelengths, are stacked to form a two-color detector, the applied bias voltage is distributed between the two based on their dynamic resistance at a given voltage. If the resistance of the short wavelength QWIP is much higher at low bias, the applied bias will be mostly across the short wavelength QWIP at low bias. When the bias is increased, the dynamic resistance of the long wavelength QWIP becomes higher than that of the short wavelength QWIP, leading the applied bias to distribute across the long wavelength QWIP. It is this same effect that leads to the interplay between the applied biases in the detector reported in this Letter. Under low bias, as shown in Fig. 2(b), the applied bias applies across the *p*-QWIP (short wavelength), while the *n*-QWIP (long wavelength) turns on at high bias as shown in the band diagram in Fig. 2(c). Although the MIR detection is prominent for forward bias, a response for very high reverse bias voltages (near the breakdown voltage) can be observed similar to forward bias, since the high leakage current refills the well ground state. The D^* values at 8.9 μm are 8.8×10^{10} and 5.1×10^{10} Jones at 80 K under 15 and -40 V bias voltages, respectively, while 5 μm peak exhibits a D^* of 1×10^{11} Jones at 80 K under 10 V bias.

As shown in Fig. 4(b), the response at 8.9 μm is sensitive to *p*-polarized light (perpendicular to the metal strips in the grating), as expected for an *n*-QWIP, while the peak at 5 μm is not sensitive to the polarization of the light, which is due to the fact that the hole transitions (5 μm peak) do not obey the polarization selection rules. The polarization extinction ratio for the 8.9 μm peak is ~100:25, and it is reasonably consistent with standard QWIPs with similar measurement geometry. The polarization extinction ratio could be further improved by using metal grids with grid periods in the 0.5–1 μm range, where polarization properties of the metal grid as well as the quantum well would contribute to the extinction ratio.

In summary, a GaAs/AlGaAs based detector was reported showing multiple capabilities. A response in the 200–870 nm range (UV/VIS) was observed for forward bias, while a response in the 590–870 nm range (VIS) was observed for reverse bias. Two MIR peaks at 5 and 8.9 μm were observed for low (10 V) and high (15 V) forward bias voltages, respectively. Furthermore, the peak at 8.9 μm exhibits polarization sensitivity with a polarization extinction ratio of 100:25.

This work is supported in part by the U.S. Air Force Office of Scientific Research (AFOSR) under STTR contract FA9550-09-C-0106 and the U.S. National Science Foundation (NSF) under contract ECS 05-53051. The authors acknowledge fruitful discussions with V. Apalkov.

References

1. H. C. Liu and F. Capasso, *Intersubband Transition in Quantum Wells: Physics and Device Applications I (Semiconductors and Semimetals)* (Academic, 2000), Vol. 62.
2. M. P. Touse, G. Karunasiri, K. R. Lantz, H. Li, and T. Mei, Appl. Phys. Lett. **86**, 093501 (2005).
3. C. J. Chen, K. K. Choi, W. H. Chang, and D. C. Tsui, Appl. Phys. Lett. **72**, 7 (1998).
4. S. D. Gunapala, S. V. Bandara, J. K. Liu, J. M. Mumolo, C. J. Hill, S. B. Rafol, D. Salazar, J. Woolaway, P. D. LeVan, and M. Z. Tidrow, Infrared Phys. Technol. **50**, 217 (2007).
5. H. C. Liu, C. Y. Song, A. Shen, M. Gao, Z. R. Wasilewski, and M. Buchanan, Appl. Phys. Lett. **77**, 2437 (2000).
6. S. Krishna, S. Raghavan, G. von Winckel, A. Stintz, G. Ariyawansa, S. G. Matsik, and A. G. U. Perera, Appl. Phys. Lett. **83**, 2745 (2003).
7. S. Chakrabarti, X. H. Su, P. Bhattacharya, G. Ariyawansa, and A. G. U. Perera, IEEE Photon. Technol. Lett. **17**, 178 (2005).
8. R. C. Jayasinghe, G. Ariyawansa, N. Dietz, A. G. U. Perera, S. G. Matsik, H. B. Yu, I. T. Ferguson, A. Bezinger, S. R. Laframboise, M. Buchanan, and H. C. Liu, Opt. Lett. **33**, 2422 (2008).
9. J. S. Tyo, D. L. Goldstein, D. B. Chenault, and J. A. Shaw, Appl. Opt. **45**, 5453 (2006).
10. S. Adachi, Phys. Rev. B **35**, 7454 (1987).
11. M. A. Khan, J. N. Kuznia, D. T. Olson, J. M. Van Hove, M. Blasingame, and L. F. Reitz, Appl. Phys. Lett. **60**, 2917 (1992).
12. H. C. Liu, J. Li, J. R. Thompson, Z. R. Wasilewski, M. Buchanan, and J. G. Simmons, IEEE Electron Device Lett. **14**, 566 (1993).